ANNALS OF GEOPHYSICS, 56, 6, 2013, S0679; doi:10.4401/ag-6208

Special Issue: Earthquake geology

Morphotectonics of the Padul-Nigüelas Fault Zone, southern Spain

Jochen Hürtgen, Andreas Rudersdorf*, Christoph Grützner, Klaus Reicherter

RWTH Aachen University, Neotectonics and Natural Hazards, Aachen, Germany

Article history
Received September 27, 2012; accepted November 18, 2013.
Subject classification:
Padul-Nigüelas Fault Zone, Fault activity, Morphotectonics, Geomorphic index, Granada Basin.

ABSTRACT

The Padul-Nigüelas Fault Zone (PNFZ) is situated at the south-western mountain front of the Sierra Nevada (southern Spain) in the Internal Zone of the Betic Cordilleras and belongs to a NW-SE trending system of normal faults dipping SW. The PNFZ constitutes a major tectonic and lithological boundary in the Betics, and separates the metamorphic units of the Alpujárride Complex from Upper Tertiary to Quaternary deposits. Due to recent seismicity and several morphological and geological indicators, such as preserved fault scarps, triangular facets, deeply incised valleys and faults in the colluvial wedges, the PNFZ is suspected to be a tectonically active feature of the south-eastern Granada Basin. We performed morphotectonic GIS analyses based on digital elevation models (DEM, cell size: 10 m) to obtain tectonic activity classes for each outcropping segment of the PNFZ. We have determined the following geomorphic indices: mountain front sinuosity, stream-length gradient index, concavity index and valley floor width to height ratio. The results show a differentiation in the states of activity along the fault zone strike. The western and eastern segments of the PNFZ indicate a higher tectonic activity compared to the center of the fault zone. We discuss and critically examine the comparability and reproducibility of geomorphic analyses, concluding that careful interpretation is necessary, if no ground-truthing can be performed.

1. Introduction

The Padul-Nigüelas Fault Zone (PNFZ) is located at the southwestern border of the Sierra Nevada in southern Spain (Figure 1) and comprises a strongly segmented northwest-southeast trending system of normal faults that dip to the southwest. Several authors have already studied the tectonic and seismic activity of the PNFZ as a separated part of the Granada Basin [Riley and Moore 1993, Keller et al. 1996, Calvache et al. 1997, Alfaro et al. 2001, Ruiz et al. 2003, 2007, El Hamdouni et al. 2008]. It is suspected to be a tectonically active region due to its recent low to moderate seismicity and several morphological and geological indicators, such as preserved fault scarps both in bedrock and in alluvial fans, triangular facets, deeply incised channels and hanging valleys (Figure 2). Nevertheless, only a few paleoseismological records of a paleo-earthquake or any historical earthquake reports have been found up to now [Alfaro et al. 2001]. Peláez Montilla et al. [2001] and Sanz de Galdeano et al. [2003] have already classified the seismic potential of active faults in the Granada Basin, our aim is to semi-quantitatively assess the activity of the PNFZ. Analyses of geomorphic indices offer an appropriate method to obtain quantitative data concerning the seismogenic potential of a fault zone in a specific area. Some studies have analyzed morphotectonics for areas of 300 km^2 to 2500 km^2 in southern Spain [Silva et al. 2003, El Hamdouni et al. 2008, Pérez-Peña et al. 2010, Azañón et al. 2012, Giaconia et al. 2012]. We selected the morphotectonic approach in a smaller scale by choosing a relatively narrow area around the main faults of the PNFZ, which corresponds to an area of approximately 200 km^2. Since the PNFZ does not consist of one particular fault, but comprises a fault zone consisting of three segments, we are interested in the tectonic activity of each segment and if there is a differentiation between each segment. This information is crucial for determining the seismic potential of the fault zone.

2. Geology and tectonic setting

2.1. Betic Cordilleras

The WSW-ENE striking Betics make up the westernmost part of the Alpine chain, and are a result of the collision of the Eurasian and African plates in N-S/NW-SE direction [Sanz de Galdeano 1990, Morales et al. 1999]. The Betic Cordilleras are made up of two main domains, the Internal and the External zones (Figure 1B). Non-metamorphic Mesozoic and Paleogene units of the External Zone form the northern and

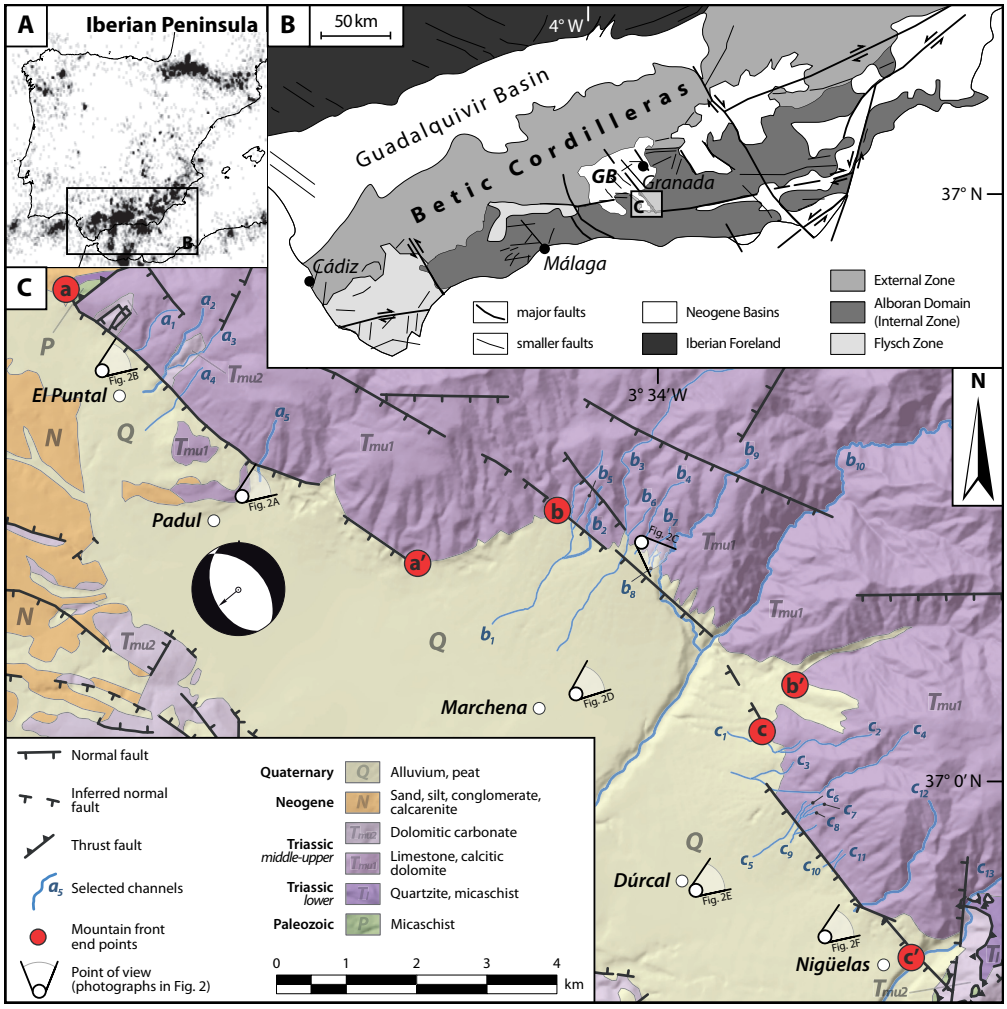

Figure 1. [A] Earthquake point density map of the Iberian Peninsula, based on USGS earthquake data (1973-2013, M>0) [B] Generalized geological map of southern Spain with the main geological units, and major fault systems. The extent of the map is marked in [A]. GB: Granada Basin (after Reicherter and Peters [2005]). [C] Simplified geological map of the Padul-Nigüelas Fault Zone (PNFZ) including the position of hardrock faults, other faults and the major lithological units in the surrounding area of the PNFZ, compiled from own data and published geological maps [Sanz de Galdeano et al. 1975, González Donoso et al. 1978]. The end points of the lines for the calculation of the mountain front sinuosity (S_{mf}) are plotted as red dots and mark the Padul (a-a'), Marchena (b-b') and Dúrcal (c-c') segments. Used channels ($a_{1\text{-}5}$, $b_{1\text{-}10}$, $c_{1\text{-}13}$) for the morphotectonic analysis (see Figures 3-5) are plotted as blue lines. The fault plane solution is taken from Muñoz et al. [2002] and based on microtectonic measurements. The extent of the map is marked in [B]. Additionally, the viewing locations for the field photographs presented in Figure 2 are indicated.

north-western parts of the Cordilleras. The Internal zone consists of three allochthonous complexes, which were tectonically superimposed and underwent (partly intense) folding, thrusting, and metamorphism. From bottom to top these complexes are Nevado-Filábrides, the Alpujárrides, and the Malaguides [Sanz de Galdeano and Alfaro 2004]. The Nevado-Filábride complex consists of schists, metamorphosed carbonates, and marbles (Alpine metamorphism of Paleozoic and Mesozoic marine sediments). The Alpujárrides comprise carbonate rocks of Lower to Upper Triassic age, which were affected by metamorphism during the Alpine orogeny (schists and marbles). The Malaguides encompass Variscan basement and a Mesozoic cover [Weijermars 1991, Vissers et al. 1995, Sanz de Galdeano and Lopez-Garrido 1999, Azañon et al. 2002, Reicherter and Peters 2005]. Flysch nappes are present in the western part of the Betic Cordilleras (Cretaceous to Early Miocene; Reicherter et al. [1994]).

2.2. Granada Basin

The intramontane Granada Basin, whose southeasternmost part comprises the study area, is bordered to the east by the prominent NW-SE striking PNFZ and other sets of faults striking subparallel to NNE-SSW. In the west, E-W structures mark the basin's southern boundary. The Granada Basin hosts the most recent rocks. Sediment thicknesses reach more than 1000 m in its central part and around 500 m at the margins. Marine sediments (mostly calcarenites and marls) were deposited during the Tortonian, then continental sedimentation prevailed and conglomerates, sandstones and marlstones were emplaced. After an evaporitic phase in the Messinian, lacustrine limestones and ter-

rigenous sandstones could form until Pliocene. Conglomerates and sands make up the youngest units of the basin (see Reicherter and Peters [2005] and references therein).

In the SE Granada Basin, NW-SE striking faults with normal movement offset the Triassic Alpujárride basement dolomites in the NE against unconsolidated sedimentary rocks in the SW (Figure 1C). Subparallel to parallel striking faults form a graben system, whose southwestern part is less developed. The hanging wall sediments include alluvial clays, sands and gravels (Red Formation, Early to Middle Pleistocene after Alfaro et al. [2001]) overlaying Upper Miocene sedimentary rocks. The top of the succession is built up by conglomerates of the Nigüelas Formation with pebbles mostly derived from Nevado-Filábridan and Alpujárridan material. Recent alluvial fans and peat deposits (Late Pleistocene to Holocene), especially in the area of Padul and La Turbera, make up the uppermost units (after Sanz de Galdeano and López-Garrido [1999], Alfaro et al. [2001]).

2.3. Tectonic background and seismicity

Neogene intramontane basin formation began due to a radial-extensional regime from Tortonian to Plio-Pleistocene [Fernández et al. 1996]. Major faults (normal and strike-slip) controlled the basin formation [Galindo-Zaldívar et al. 1993, 1999, Sanz de Galdeano and Lopez-Garrido 1999, Martínez-Martínez et al. 2006]. The Granada Basin is slightly tilted towards the N.

Recent tectonic movements are mainly driven by a NW-SE directed maximum horizontal stress, with σ_1 being vertical and σ_3 having a NE-SW orientation in most cases [Galindo-Zaldívar et al. 1993, 1999, Herraiz et al. 2000]; however, regional deviations from that general setting can be observed (radial extension, NE-SW extension; see Galindo-Zaldívar et al. [1993]). Normal faulting dominates the central part of the Betic Cordilleras, but minor strike-slip movements can also be observed. Sanz de Galdeano [1990] reports the main fault patterns to be NW–SE, NE–SW, NNE–SSW and E–W (see also Reicherter and Peters [2005] and references therein), which is in accordance with the recent stress field. N(N)E-S(S)W extension is characteristic for the study area. East of the PNFZ, NNE-SSW striking normal faults show a strike-slip component. The PNFZ strikes parallel to the recent maximum horizontal stress and this direction permits movements as normal fault, facilitating the extension parallel to the minimum horizontal stress.

Present day seismicity is among the highest on the Iberian Peninsula [Mezcua et al. 2013] (Figure 1A). The plate boundary between Nubia and Iberia is seismically rather undefined and seismic events are scattered over a broad region. Instrumental, historical, and paleoseismological records prove that significant earthquakes have occurred in the Granada Basin, some of which have been destructive events [Reicherter 2001]. Basin-wide paleoseismic information is scarce and recurrence intervals are often unknown [Sanz de Galdeano et al. 2003]. The best-known event nearby is probably the 1884 Arenas del Rey earthquake (or Andalusian earthquake) that occurred at the Ventas de Zafarraya fault in the SW Granada Basin and caused several hundred casualties. It had a magnitude of M>6.5. The Ventas de Zafarraya Fault is likely to have a recurrence interval of 2-3 ka [Reicherter et al. 2003, Grützner et al. 2013]. Few shallow events in Andalusia may reach magnitudes of more than 6.3, judging from the fault lengths and empirical ratios [Wells and Coppersmith 1994]. For the larger faults, no instrumental record of events > M6.3 is available. Paleoseismological or archeoseismological data do not often clearly point to much stronger events, and recurrence intervals for very strong events are long. Stronger but very deep-seated events (>600 km depth) occurred in the study area (e.g. M7.0, 1954; M6.3, 2010) and are most likely related to the subduction of oceanic crust below Iberia in the Gibraltar subduction arc. Due to their depth, they do not significantly contribute to the seismic hazard of Andalusia. Small minor events (M<5.5) occur frequently within the region. Overall, a moderate seismicity can be assigned to the Granada Basin.

2.4. The Padul-Nigüelas Fault Zone (PNFZ)

In sensu stricto the PNFZ comprises two faults: the first is the 15 km long Padul Fault, which extends from the East of La Malahá to the village of Marchena [Sanz de Galdeano and Peláez 2010a] and crops out for circa 5 km. The second fault is the 13 km long Nigüelas or Padul-Dúrcal Fault [Sanz de Galdeano and Peláez 2010b], which extends from N of El Puntal to Nigüelas and strikes partly within the Alpujárride units, subparallel to the Padul Fault. Both faults are sub-parallel and dip to the SW. Slip rates are estimated to be between 0.16 to 0.35 mm/a and 0.2 to >0.35 mm/a, respectively, with no horizontal component. Maximum moment magnitudes are in the order of M_w 5.9-6.6 and M_w 5.9-6.5 (after empirical rupture length relationships, see Wells and Coppersmith [1994]), and M_w 6 earthquake recurrence intervals of <1200a and <1300a for normal movements of the Padul Fault and Nigüelas Fault are reported, respectively [Sanz de Galdeano et al. 2003, Sanz de Galdeano and Peláez 2010a, 2010b]. There are no instrumental recordings of significant earthquakes at the PNFZ. Nearby events are characterized by focal mechanisms that are in good agreement with the overall tectonic setting [Muñoz et al. 2002]. Additional fault characteristics are compiled in

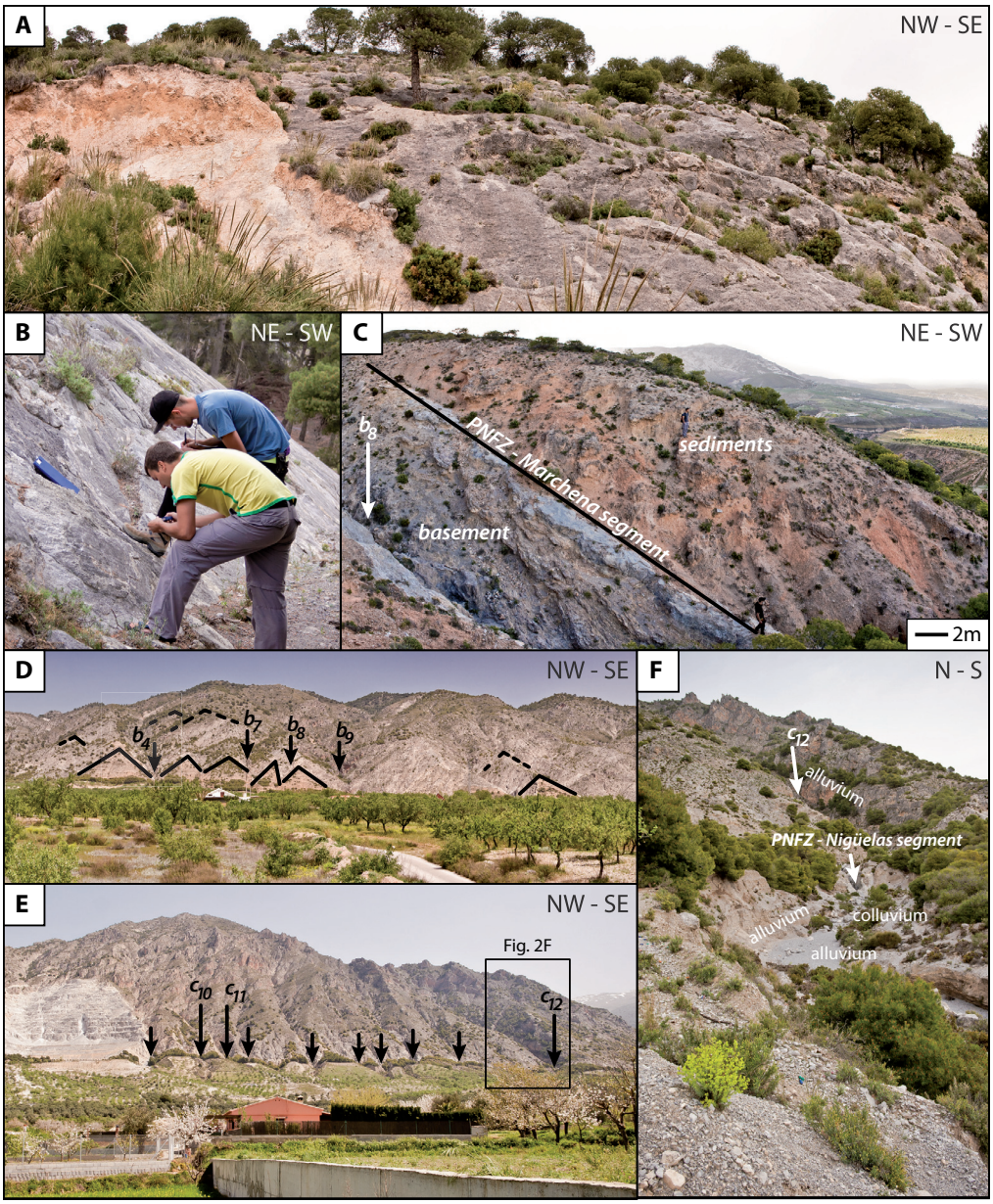

Figure 2. Field photographs from the study area. Orientation is indicated by the cardinal directions, view direction is plotted in Figure 1. [A] Bedrock fault scarp with different levels of degradation in the south-eastern part of the Padul segment. [B] Measuring dips and dip directions at the north-western part of the Padul segment. [C] Contact of the Alpujárride basement fault and the Neogene and Quaternary sedimentary overlay in *channel* b_8 (see [D] for location). [D] Different generations of triangular facets at the Marchena segment (solid black lines: youngest facets; dashed black lines: older generations). Black arrows indicate the position of *channels* b_4, b_7, b_8 and b_9. [E] Triangular facets and incised channels (black arrows, especially *channels* c_{10}, c_{11} and c_{12}) at the Dúrcal segment. [F] Detailed view of an incised *channel* c_{12} (see [E] for location).

the Quaternary Active Faults Database of Iberia (QAFI; García-Mayordomo et al. [2012]).

2.5. Morphological evidence

The PNFZ can be divided into several sub-segments: the outcropping Padul Fault segment in the NW, and two segments of the outcropping Nigüelas Fault: the Marchena segment in the center of the PNFZ, and the Dúrcal segment in the southeastern part (Figure 1). Since the Padul and Nigüelas segments are related to different faults, discrimination retains the possibility of assessing different fault activities. Additionally, we subdivided the Nigüelas Fault segment into the Marchena and Dúrcal segments. The latter exhibits a prominent fault scarp, polished outcrops of remarkable heights [Sanz de Galdeano et al. 2003], with the fault line visible from the distance (Figure 2E), whereas the central Marchena segment seems to be more erosion-dominated (Figure 2D) with primarily rivers and creeks cross-cutting and exhuming the fault zone (Figure 2C). Geological maps vary in the certainty of the fault line in the Marchena area [Sanz de Galdeano et al. 1975, Alfaro et al. 2001, El Hamdouni et al. 2008, Sanz de Galdeano et al. 2010b, and others], we therefore favor an independent evaluation, also following the suggestion of Burbank and Anderson [2001] to subdivide into

segments facing possible changes in lithological resistance, orientation of the range front, steps in the bounding faults, cross-cutting river valleys or significant changes in the geomorphic character.

Field observations reveal active, morphotectonic features in the study area (Figure 2). Mountain fronts of the PNFZ are characterized by different generations of triangular facets, which are separated by deeply incised channels building partially hanging valleys in close proximity to the fault zone. The PNFZ offsets mainly limestones and dolomites of the Alpujárride basement against poorly consolidated sediments of Upper Miocene and younger ages, and forms well-preserved hardrock scarps in the Padul and the Dúrcal segments. These lithologies can be found in the entire fault zone. Soft-rock sediments generally overlay the hardrock fault plane in the Marchena segment. Faulting of Pliocene and Pleistocene sediments in the alluvial fans in front of the SW mountain front of the Sierra Nevada is interpreted as synthetic faulting connected to the main fault of the PNFZ [Alfaro et al. 2001]. The three segments of the fault zone show a strong variation in dipping angle and dip direction. The dipping angles for the entire PNFZ scatter from around 20° up to 70°, whereby the dip direction varies between 180° to 260°. This data is based on our own field measurements on the hardrock fault plane of the PNFZ. In spite of the undulating fault segment, the mountain fronts of the western (Padul segment) and eastern parts (Dúrcal segment) of the PNFZ are relatively straight with a mean dip direction of 215° (± 17°) for the Padul segment and 236° (± 14°) for the Dúrcal segment. In contrast, a more sinuous shape characterizes the mountain front of the Marchena segment with a mean dip direction of 220° (± 24°). The hardrock fault plane dips in the Padul and Dúrcal segment with angles of 47° (± 11°) and 50° (± 3°), whereas the Marchena hardrock fault plane has a shallower dipping angle of 35° (± 12°). Most of the alluvial fans ahead of the mountain fronts of the Padul and Dúrcal segments are steep, whereas the Marchena segment is characterized by a broad and wide fan with gentle slopes. Other morphological features like triangular facets, incised channels and hanging valleys strongly support a relevant recent tectonic activity and create a seismic landscape in the sense of Michetti et al. [2005].

3. Methods

For our morphotectonic analyses we compiled a data set in a Geographic Information System (GIS) including geological maps, several aerial photograph series from the 1950s, 2004 and 2009, and vectorized data from the Junta de Andalucía *Line@* online database (v.1: ICA [2011], now v.2: IECA [2013]), the latter of which contains digitized 10 m contour lines of the 1:10,000 topographic map. From this data a digital elevation model (DEM) was created, which made it possible to get detailed topographic information for the analyses of morphotectonic features along the PNFZ. Several studies describe how analyses of morphometric features in profiles along rivers and mountain fronts can be used to determine regional tectonic activity [Wells et al. 1988, Riley and Moore 1993, Calvache et al. 1997, Kirby and Whipple 2001, Silva et al. 2003, El Hamdouni et al. 2008, Larue 2008, Pérez-Peña et al. 2010]. We use four different geomorphic parameters (mountain front sinuosity S_{mf}, stream-length gradient index *SL*, concavity index A_c and valley floor width to height ratio *Vf*) to evaluate the tectonic activity and to classify each segment of the fault. Not only are these parameters well documented in the literature, but they can also easily be calculated in the study area.

3.1. Concavity index

To determine the concavity of a stream profile, a concavity index can be quantified by the area A_c under the normalized channel profile [Wells et al. 1988]. The normalization is done by dividing the elevation by the total basin relief and by dividing the distance by the total length of the profile. Channels in an equilibrium stage have lower concavity values, whereas rivers in tectonically active regions result in higher concavity indices [Wells et al. 1988, Kirby and Whipple 2001, Figueroa and Knott 2010].

$$A_c = \sum_{i=1} \frac{h_i + h_{i+1}}{2}(l_{i+1} - l_i)$$

The equation calculates the area under the segmented normalized channel profile by summing up each single area under the trapezoid segment with h = normalized elevation; l = normalized distance from source.

3.2. Stream-length gradient index

The development of the morphology of a landscape is highly influenced by the interaction between erosional processes and tectonic-induced phenomena, such as uplift of a region. These changes can be identified in channel profiles and can be quantified by the stream length-gradient index *SL*. The *SL* index was firstly introduced by Hack [1973] and is defined as:

$$SL = \frac{\Delta H}{\Delta L} L$$

The total longitudinal profile of a river or channel is divided into DEM cell-sized segments. ΔH is the ele-

vation difference for one grid cell and ΔL is the corresponding length of this segment. L is the total channel length from the midpoint of the segment where the SL value is calculated upstream to the divide. The value of the SL index will increase as rivers flow over active uplifted areas [Keller and Pinter 2002].

3.3. Valley floor ratio

The valley floor ratio Vf (or valley floor width to height ratio) distinguishes different shapes of valleys that can be interpreted as possible indications for tectonic activity. High values of Vf are connected to "U" shaped valleys, which have relatively wide valley floors. The "V" shape of a valley is represented by low values of Vf, which are associated with strong incision rates. In a state of equilibrium, incision rates are strongly connected to the uplift of an area; this can be interpreted as an indication for tectonic activity.

$$Vf = \frac{2w_{vf}}{(E_{ld} - E_{sc}) + (E_{rd} - E_{sc})}$$

The Vf index is defined as the ratio of the width of a valley floor w_{vf} to its average height. This is calculated using the elevation of the left drainage divide of the investigated valley E_{ld}, the elevation of its right drainage divide E_{rd}, and the average elevation of the valley floor E_{sc} [Bull and McFadden 1977]. It is crucial to investigate comparable survey points and, therefore, determine reproducible positions, e.g. fixed distances upstream from a mountain front, sink or lithological boundary.

3.4. Mountain front sinuosity

The tendency of active tectonic structures to influence and overprint surface morphology by maintaining rather straight (fault) lines opens the possibility to investigate intersections of mountain ranges with basin structures. Tectonically inactive structures, in contrast, exhibit highly irregular and lobate landforms, dominated by erosional processes. Bull and McFadden [1977] introduced mountain front sinuosity S_{mf}, which is defined by the ratio of the mountain front piedmont intersection L_{mf}, where a significant change in slope from the mountain to the piedmont occurs, to the straight line distance along the mountain front L_s [Bull and McFadden 1977, Burbank and Anderson 2001, Bull 2007]:

$$S_{mf} = \frac{L_{mf}}{L_s}$$

Values of S_{mf} close to 1.0 correspond to tectonically active mountain fronts, whereas inactive mountain fronts show much higher values up to 7.0 [Bull and McFadden 1977].

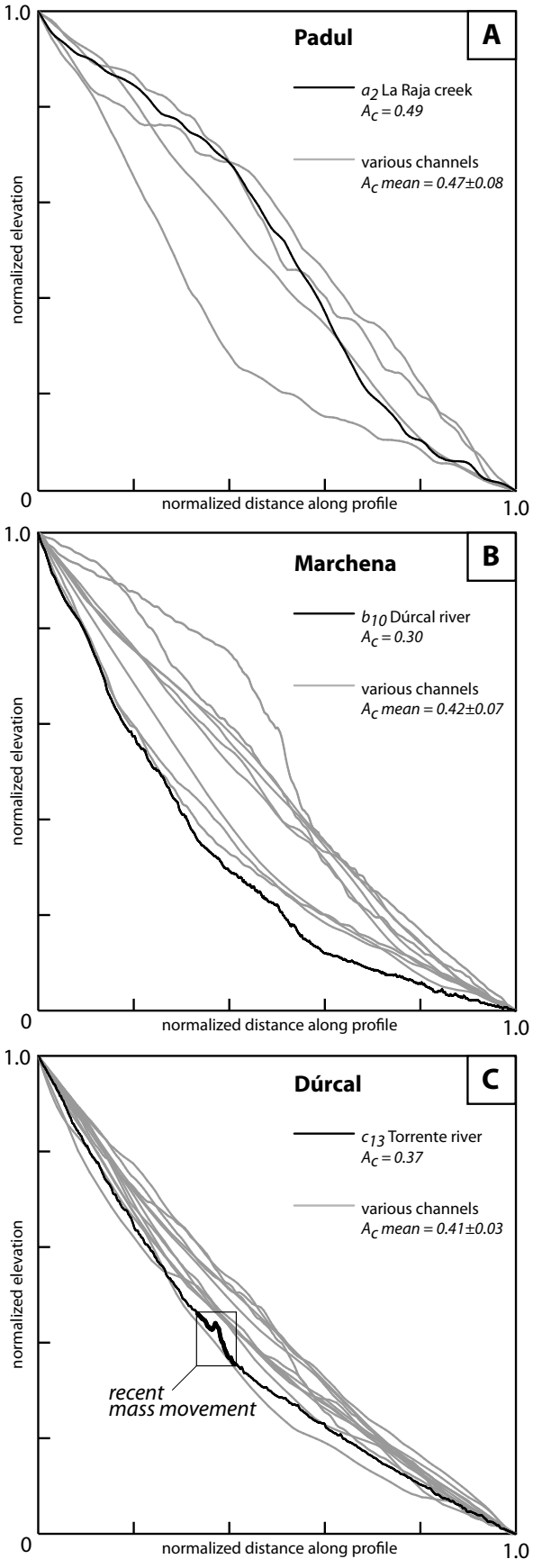

Figure 3. Combined concavity index plots for the three segments of the PNFZ ([A] Padul, [B] Marchena and [C] Dúrcal). One of the used channels for each segment (a_2, b_{10}, c_{13}) is plotted as thick line. In the graph, the mean value for all channels of each segment is given. See Figure 1 for location of channels and Table 2 for the derived values of A_c.

4. Results

4.1. Concavity index

The profiles for the concavity index A_c are plotted in Figure 3 separately for each segment. The number of selected channels in each segment varies due to the occurrence and the length of the available channels. The values of the concavity index indicate different distribution patterns for the three segments of the PNFZ. In the Padul segment (see Figure 3A), only five channels comply with the requirement of crossing the fault zone and, therefore, only these are selected for analyzing the concavity index. The mean value in this segment indicates the highest A_c values around 0.47 with a standard deviation of ±0.08. The highlighted La Raja creek shows a very high value in the concavity index (0.49). These higher values are only reached in the western segment. Similar to the variation of the values in

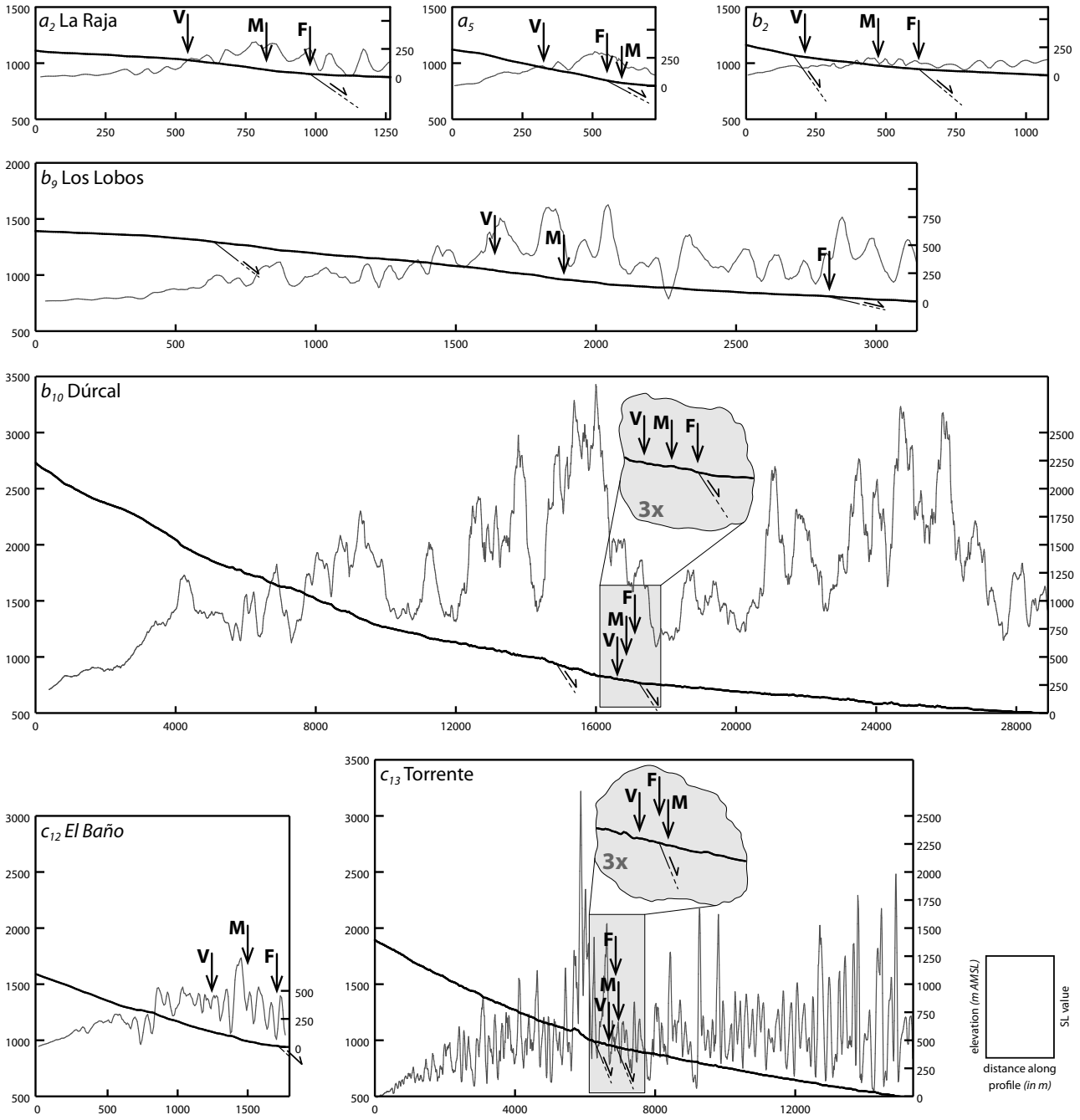

Figure 4. Calculated stream-length gradient index SL (gray line) for selected channel profiles (thick black line). Black arrows indicate the position of the mapped main fault of the PNFZ (F), the mountain front (M) and the valley floor measurements (V). Additionally, the position of nearby faults is indicated in the profiles. See Figure 1 for location of channels and Table 2 for the calculated values of *SL*. Profiles a_2, a_5, b_3 and b_9 are 2.5x reduced in vertical scale; Profile c_{12} is 1.25x reduced in vertical scale and profiles b_{10} and c_{13} are 3x vertically exaggerated. See lower right box for units.

the Padul area, the standard deviation for the concavity index is ±0.07 in the Marchena segment. Generally, the mean concavity index for this segment is lower (0.42) compared to the Padul segment, whereas the Dúrcal river (see Figure 3B) reaches only a value of 0.30, which describes a mature fluvial stream system. The A_c values for the Dúrcal segment (see Figure 3C) indicate a narrow distribution around a mean value of 0.41 with a low standard deviation of ±0.03. Regarding the concavity and compared to the western and central segment, the development of the channels in the eastern part of the PNFZ seems to be relatively homogeneous.

4.2. Stream-length gradient index

To assess slope gradient irregularities we investigated 28 both permanently and episodically water-bearing channel profiles of different lengths across the PNFZ. Ideally, a river maintains a smooth slope from source to sink, hence peaks in *SL* plots represent irregularities or knick points, which are due to lithology changes, mass movements (especially for episodic rivers) and fault movements. In combined plots (Figure 4), *SL* peaks can easily be linked to topographic features. Nevertheless, DEM inconsistencies increasingly influence the smoothness of *SL* lines where there are gentle slopes or flat basin areas and may lead to misinterpretations.

To visualize *SL* values, we selected seven characteristic channels distributed throughout all segments of the PNFZ (Figure 1c). La Raja creek (Figure 4, a_2), with episodic water flow, is a deeply incised channel and crosses the Padul fault segment. The channel profile is smooth with gradually rising, low anomalous *SL* values and wide *SL* peaks, which coincide with the mountain front and the fault trace, respectively. The short channel a_5 (Padul segment, Figure 4, a_5) shows a significant wide bulging peak, whereas channel b_2 (Marchena segment, Figure 4, b_2) exhibits only insignificant *SL* values with no characteristic peaks. The Los Lobos creek and Dúrcal river (Marchena segment, Figure 4, b_9 and b_{10}) are characterized by higher water flow rates. Here, *SL* anomalies are higher and abrupt changes in topography can be clearly traced. We observe high anomalies in the Dúrcal segment at the El Baño creek and the Torrente river (Figure 4, c_{12} and c_{13}), where a non-tectonic structure produces the most characteristic peak; a recent mass movement body in the Torrente valley, triggered by fluvial erosion, provides evidence for irregular slope angles and hence a very high *SL* peak.

4.3. Valley floor ratio

The valley floor ratio *Vf* is used to assess the shape of valleys and to draw conclusions regarding their incision rates. The incision rate of flowing water is linked to multiple factors like flow rate, sediment transport and lithology, but also to the regional tectonic uplift rate. Incision-dominated valleys are V-shaped and produce low valley floor ratios, whereas high valley floor ratios are derived from U-shaped valleys, which are sedimentation-dominated. Since all investigated channels flow through similar lithologies, the calculated *Vf* of twenty channels, measured at a distance of 250 m from the mountain front, can be easily compared.

In the Padul segment *Vf* values range between $V_{f\,min}$=0.75 and $V_{f\,max}$=1.49, in the Marchena segment between $V_{f\,min}$=0.10 and $V_{f\,max}$=2.00, and in the Dúrcal segment between $V_{f\,min}$=0.09 and $V_{f\,max}$=3.11. For consistency, short channels that do not exceed 250 m above the mountain front were not considered in any of the *Vf* calculations. In Figure 5, seven exemplary valley floor profiles show the variety of valley shapes through-

Tectonic Activity Class		Bull and McFadden [1977]	Rockwell et al. [1985]	Silva et al. [2003]	El Hamdouni et al. [2008]
I	S_{mf}	1.2-1.6	<1.4	<1.53	<1.1
	Vf	0.055-0.5	<1	<0.6	<0.5
	SL	-	-	-	high anomalies
II	S_{mf}	1.8-3.4	-	1.8-2.3	1.1-1.5
	Vf	0.5-3.6	-	0.3-0.8	0.5-1
	SL	-	-	-	low anomalies
III	S_{mf}	2-7	>1.4	2.8-3.5	>1.5
	Vf	2-47	>1	0.8-1.2	>1
	SL	-	-	-	no anomalies

Table 1. Overview of tectonic activity classes compiled by Bull and McFadden [1977], Rockwell et al. [1985], Silva et al. [2003], El Hamdouni et al. [2008]. These ranges are used to classify each value of geomorphic indices in Table 2 and to conclude on a tectonic activity class for each of the three segments of the PNFZ.

out the PNFZ. We encountered different clusters of shapes: valleys in the Padul segment (a_2, a_5) are broader and the valley floors and shoulders have low elevation differences; valleys in the Marchena segment are steeper (b_2, b_9, b_{10}); and the investigated valleys in the Dúrcal segment (c_{12}, c_{13}) are asymmetric, with the Torrente valley (c_{13}) being characterized by a wide valley floor. The asymmetric valleys are likely caused by structural weaknesses: the tipping Nigüelas fault being crosscut by conjugate and oblique faults.

In the PNFZ, V-shaped and therefore incision-dominated valleys, are common and represent an active erosional environment. However, the valley floor ratio is not capable of differentiating underlying processes.

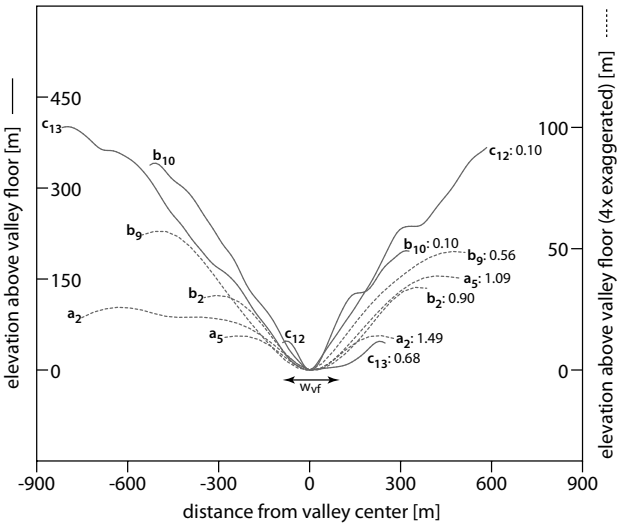

Figure 5. Valley-floor ratio for selected channels (a_2, a_5, b_2, b_9, b_{10}, c_{12}, and c_{13}). The solid profile lines are plotted without exaggeration; the dashed lines are four-time vertically exaggerated. Calculated valley-floor ratios are given at the right side of each profile. See Figure 1 for location of the channels and Table 2 for calculated values of *Vf* for all channels.

4.4. Mountain front sinuosity

We have distinguished three segments on the PNFZ, which are shown on the map in Figure 1c, as the Padul segment (a-a'), the Marchena segment (b-b') and the Dúrcal segment (c-c'), based on remote sensing and field observations. The mountain front north of Padul seems to be directly connected to the Padul Fault (Figure 1), whereas the other segments can be related to the Nigüelas Fault. Nevertheless, the latter exhibits a two-part habitus. The northwestern part shows a highly irregular mountain front with previously unclear fault line trends [Sanz de Galdeano et al. 1975, González Donoso et al. 1978]. In contrast, the southeastern part seems to be directly linked to the Nigüelas Fault. The straight mountain front lines L_{mf} were semi-automatically determined on the DEM, using a combination of a distinct change in slope and the aspect ratio. To compensate areas of anthropogenic overprinting by e.g. quarries, we there omitted the semi-automatic determination and consulted aerial photographs from the late 1950s that show natural mountain front trends.

The straight line distances L_s of the three segments vary in length from circa 3 to 5 km. For the Padul and Nigüelas segments the S_{mf} values are low (S_{mf} = 1.34), whereas the Marchena segment has a higher S_{mf} value of 1.65. The mountain fronts of the Padul and Dúrcal segments are relatively straight and only influenced by smaller, intermittently water-bearing channels. The Río Dúrcal and the parallel channels of Los Lobos mainly cause the higher S_{mf} value of the Marchena segment due to retrogressive incision and erosion.

4.6. Activity classes

The classification of indices is a sensitive step in the process of judging tectonic activity. Biased class limits hold the danger of falsifying results by over- or underestimation. Hence, we used published classifications for orientation; Table 1 provides a synopsis of regional class limits after Bull and McFadden [1977], Rockwell et al. [1985], Silva et al. [2003] and El Hamdouni et al. [2008], Table 2 provides all measured data of this study. We rescinded from developing our own classes but combined evaluations after previous authors and present averaged results by calculating the arithmetic mean. All classifications are subdivided in three sub-classes: class I represents the highest tectonic activity level, class II corresponds to a moderate tectonic activity level, and class III characterizes low or absent tectonic activity. These classifications are designed to quantify morphological and hence highly irregular features that are difficult to compare. Since most published classifications are limited to the respective regional lithologies, recent geologic history, climate and weathering conditions, existing classifications have to be implemented carefully.

In this study, we consider three different segments in the PNFZ and derive diverse activity ratings (Table 2). The stream length gradient index rating shows class I-II activity in the Padul and Dúrcal segments (mean rating: 1.7), whereas ratings are lower in the Marchena segment (class II, mean rating: 2.0). The valley floor ratio rating, in contrast, results in class II-III activity for the Padul segment (mean rating: 2.55), with increasing ratings toward the east; an intermediate class II activity is ascribed to the Marchena segment (mean rating: 1.92), and class I-II activity is registered for the Dúrcal section (mean rating: 1.83). The mountain front sinuosity rating again shows high activity ratings for the Padul and Dúrcal segments with both segments having class I ratings (mean rating: 1.25), whereas the Marchena segment exhibits low activity ratings (mean rating: 2.13).

	Name		Concavity	Stream length gradient index					Valley floor ratio								Mountain front sinuosity							Qualitative activity rating[3]	Activity class
			A_c	$\overline{SL}$	σ	ΔH [m]	ΔL [m]	Tectonic activity[4]	Vf	ΔH_R [m]	ΔH_L [m]	d_{vf} [m]	A[1]	A[2]	A[3]	A[4]	S_{mf}	L_s	L_{mf}	A[1]	A[2]	A[3]	A[4]		
Padul	a_1.	Channel	0.53	79	72	148	750	I	1.25	46.6	30.9	48.4	II	III	III	III									
	a_2.	La Raja	0.49	117	91	236	1262	II	1.49	25.8	14.1	29.7	II	III	III	III									
	a_3.	Channel	0.53	100	81	187	1027	II	0.75	41.9	63.9	39.9	II	I	II	II	1.36	3293	4492	II	I	I	I	I-II (1.67)	I-II (1.79)
	a_4.	Channel	0.33	69	40	204	987	II	1.04	2.8	16.4	10.0	II	III	III	III									
	a_5.	Channel	0.49	152	82	323	730	I-II	1.09	14.0	39.2	29.1	II	III	III	III									
Marchena	b_1.	Channel	0.34	165	73	485	2609	III	0.59	12.4	51.3	19.5	II	I	I	II									
	b_2.	Channel	0.34	93	33	272	1088	III	0.9	30.7	34.0	29.0	II	I	III	II									
	b_3.	Channel	0.53	335	302	623	4784	I	0.21	104.4	84.1	19.5	I	I	I	I									
	b_4.	Channel	0.45	164	98	365	1042	I	0.99	13.0	46.6	19.9	II	I	III	II									
	b_5.	Channel	0.43	61	34	144	420	I	1.44	7.7	6.1	9.9	I	III	III	III									
	b_6.	Channel	0.45	76	44	168	419	I	2.00	3.7	6.2	10.0	II	III	III	III	1.65	3343	5508	III	III	I	I-II	II (1.93)	II (2.0)
	b_7.	Channel	0.46	95	55	209	519	III	1.27	5.9	9.3	9.6	II	III	III	III									
	b_8.	Channel	0.37	36	15	96	295	III	too short																
	b_9.	Los Lobos	0.48	305	192	629	3147	II	0.56	57.1	48.8	29.6	II	I	I	II									
	b_{10}.	Dúrcal	0.30	1068	554	2248	28899	II	0.10	398.2	196.5	29.8	I	I	I	I									
Dúrcal	c_1.	Channel	0.45	99	57	217	967	II-III	1.29	32.8	74.7	69.4	II	III	III	III									
	c_2.	Channel	0.41	169	82	414	1165	II	0.80	4.8	69.2	29.6	II	I	II	II									
	c_3.	Channel	0.41	58	29	140	569	I	too short																
	c_4.	Channel	0.42	275	167	657	2372	I	0.09	50.6	169.0	9.9	I	I	I	I									
	c_5.	Channel	0.40	77	34	198	917	III	too short																
	c_6.	Channel	0.39	39	19	98	228	I	too short																
	c_7.	Channel	0.35	73	34	207	521	II-III	3.11	2.9	3.2	9.6	II	III	III	III	1.34	3078	4112	II	I	I	I	I-II (1.67)	I-(II) (1.57)
	c_8.	Channel	0.43	36	17	79	153	-	too short																
	c_9.	Channel	0.37	38	20	100	377	I	too short																
	c_{10}.	Channel	0.43	59	27	137	295	II	too short																
	c_{11}.	Channel	0.40	44	18	110	249	II-III	too short																
	c_{12}.	El Baño	0.44	291	182	659	1808	I	0.09	47.4	366.6	19.8	I	I	I	I									
	c_{13}.	Torrente	0.37	561	358	1416	14269	I	0.68	447.1	49.6	169.2	II	I	II	II									

Table 2. Compilation of calculated values of all geomorphic indices. The given geomorphic values, and the activity ratings after ([1]) Bull and Mc Fadden [1977], ([2]) Rockwell et al. [1985], ([3]) Silva et al. [2003] and ([4]) El Hamdouni et al. [2008] are non-dimensional. The classification corresponds to the given ranges in Table 1; see Figure 1 for the locations of the channels.

Silva et al. [2003] add a qualitative rating to analyze and categorize structural features like assemblages of tectonic landforms, fan body interaction and paleoseismic records. We adapt the characteristic rating and also estimate a qualitative activity based on the DEM and field observations (Table 2). Since the study area is comparatively small, we derive similar results for the Padul, Dúrcal (I-II) and Marchena segments (II).

A combination of the numerous activity ratings result in a class I-II activity for the Padul and Dúrcal segments. The Dúrcal segment exhibits the most active mean rating of 1.57, whereas the mean rating of the Padul segment is slightly lower (1.79). Eventually, we are able to assess the overall tectonic activity of the PNFZ and can confirm a segmentation of the observed fault zone, which our geomorphic analyses characterize as a highly to intermediate active tectonic zone.

5. Discussion and conclusion

The mountain front sinuosity investigation resulted in medium high to high activity ratings. We developed a more solid approach in the imprecise calculation by abandoning arbitrary end points [Bull 2007] and manual mountain front delineation. We hence used major geomorphological changes, changes in the orientation of the range front and steps of the bounding faults as end-points and delineated the mountain front semi-automatically, based on DEM slope calculations. However, a leap towards complete automation remains undone and proper DEM resolution limits and investigation ruler lengths have still to be assessed.

A study by El Hamdouni et al. [2008] revealed significantly lower mountain front sinuosities (1.04-1.11) and, therefore, a more active rating. We hesitate to compare our results directly, because we cannot be sure of the determining factors confining their digital elevation model and approach. Very low values only occur with lowest deflections from straight lines and are unlikely to result from a sufficiently resolved DEM of the PNFZ, or are possibly derived from large ruler lengths. However, both our results and the values given by El Hamdouni et al. [2008] point to a tectonically active study area.

The investigation of perennial or intermittent streams gives robust information on erosion equilibria and hence points to tectonic overprinting, *inter alia*. We have thoroughly selected fluvial channels to apply concavity and valley floor indices and excluded channels from the calculation where requirements of e.g. length or size in respect to the DEM resolution were not met. The concavity indices exhibit moderate evidence for tectonically overprinted channels due to scattering distributions and partly diffuse clustering of the plots; A_c values point to medium yet overprinted river equilibrium profiles. Here, plotting the stream length gradient index together with topography and geological information is helpful to interpret unclear results and to better judge river profile disturbances. Therefore, Figure 4 shows locations of faults and helps to identify assumed fault lines. Concavity and stream length gradient indices as well as valley floor ratios provide evidence for a tectonically active study area.

Through the analysis and combined ratings of geomorphic indices we can conclude that the PNFZ is a morphotectonically active region, although both instrumental and historic seismicity is low and paleoseismologic records of the PNFZ faults (*sensu stricto*) are sparse. An additional qualitative approach to tectonic landforms after Silva et al. [2003] resulted in medium to high activity classifications for all considered segments of the PNFZ.

Morphotectonic studies help to identify tectonically active regions and open a frame for further research, for paleoseismological surveys to reveal specific slip and recurrence rates and to better understand fault behavior to eventually quantify seismic hazard.

Acknowledgements. We thank Paula Marques Figueiredo and Carlos Sanz de Galdeano for detailed, experienced and helpful comments, Jack Mason for the language improvement of the manuscript and the community of the 2nd INQUA-IGCP 567 Corinth Workshop 2011 for fruitful discussions on our research topics.

References

Alfaro, P., J. Galindo-Zaldívar, A. Jabaloy, C. Lopéz Garrido and C. Sanz de Galdeano (2001). Evidence for the activity and paleoseismicity of the Padul fault (Betic Cordillera, southern Spain), Acta Geologica Hispanica, *36*, 283-295.

Azañón, J., J.M. Galindo-Zaldívar, V. García-Dueñas and A. Jabaloy (2002). Alpine tectonics II: Betic Cordillera and Balearic Islands, In: W. Gibbons and T. Moreno (eds.), The Geology of Spain, Geological Society of London, London, 401-416.

Azañón, J.M., J.V. Pérez-Peña, F. Giaconia, G. Booth-Rea, J.M. Martínez-Martínez and M. Rodríguez-Peces (2012). Active tectonics in the central and eastern Betic Cordillera through morphotectonic analysis: the case of Sierra Nevada and Sierra Alhamilla, Journal of Iberian Geology, *38*, 225-238.

Bull, W., and L. McFadden (1977). Tectonic geomorphology north and south of the Garlock fault, California, In: D.E. Doehring (ed.), Geomorphology in Arid Regions, Proceedings 8th Annual Geomorphology Symposium, State University of New York, Binghampton, 115-137.

Bull, W. (2007). Tectonic geomorphology of mountains: a new approach to paleoseismology, Blackwell

Publishing, Malden, 119-127.

Burbank, D.W., and R.S. Anderson (2001). Tectonic geomorphology, John Wiley & Sons, 13-32, 105-130, 201-230.

Calvache, M.L., C. Viseras and J. Fernández (1997). Controls on fan development - evidence from fan morphometry and sedimentology, Sierra Nevada, SE Spain, Geomorphology, 21, 69-84; doi:10.1016/S0169-555X(97)00035-4.

El Hamdouni, R., C. Iriagaray, T. Fernández, J. Chacón and E.A. Keller (2008). Assessment of relative active tectonics, southwest border of the Sierra Nevada (southern Spain), Geomorphology, 96, 150-173; doi:10.1016/j.geomorph.2007.08.004.

Fernández, J., J. Soria and C. Viseras (1996). Stratigraphic architecture of the Neogene basins in the central sector of the Betic Cordillera (Spain): tectonic control and base-level changes, In: P.F. Friend and C.J. Dabrio (eds.), Tertiary Basins of Spain, Cambridge University Press, Cambridge, 353-365.

Figueroa, A.M., and J.R. Knott (2010). Tectonic geomorphology of the southern Sierra Nevada Mountains (California): Evidence for uplift and basin formation, Geomorphology, 123, 34-45; doi:10.1016/j.geomorph.2010.06.009.

Galindo-Zaldívar, J., F. González-Lodeiro and A. Jabaloy (1993). Stress and palaeostress in the Betic–Rif cordilleras (Miocene to the present), Tectonophysics, 227, 105-126; doi:10.1016/0040-1951(93)90090-7.

Galindo-Zaldívar, J., A. Jabaloy, I. Serrano, J. Morales, F. González-Lodeiro and F. Torcal (1999). Recent and present-day stresses in the Granada Basin (Betic Cordilleras): example of a late Miocene-present-day extensional basin in a convergent plate boundary, Tectonics, 18 (4), 686-702; doi:10.1029/1999TC900016.

García-Mayordomo, J., J.M. Insua-Arévalo, J.J. Martínez-Díaz, A. Jiménez-Díaz, R. Martín-Banda, S. Martín-Alfageme, J.A. Álvarez-Gómez, M. Rodríguez-Peces, R. Pérez-López, M.A. Rodríguez-Pascua, E. Masana, H. Perea, F. Martín-González, J. Giner-Robles, E.S. Nemser, J. Cabral and the QAFI Compilers Working Group (2012). The Quaternary Active Faults Database of Iberia (QAFI v.2.0), Journal of Iberian Geolology, 38 (1), 285-302; doi:10.5209/rev_JIGE.2012.v38.n1.39219.

Giaconia, F., G. Booth-Rea, J.M. Martínez-Martínez, J.M. Azañón, J.V. Pérez-Peña, J. Pérez-Romero and I. Villegas (2012). Geomorphic evidence of active tectonics in the Sierra Alhamilla (eastern Betics, SE Spain), Geomorphology, 145-146, 90-106; doi:10.1016/j.geomorph.2011.12.043.

González Donoso, J., V. García-Dueñas, J. Gallegos and J. Avidad Castañeda (1978). Mapa Geológico de España - 1041 Dúrcal, Instituto Geológico y Minero de España.

Grützner, C., P. Ruano, A. Jabaloy, J. Galindo-Zaldívar, P. Becker-Heidmann, C. Sanz de Galdeano, A. Rudersdorf and K. Reicherter (2013). Late Holocene rupture history of the Ventas de Zafarraya Fault (Southern Spain), Cuaternario y Geomorfología, 27 (3-4), 52-61.

Hack, J. (1973). Stream-profile analysis and stream-gradient index, USGS J. Res., 1, 421-429.

Herraiz, M., G. De Vicente, R. Lindo-Ñaupari, J. Giner, J.L. Simón, J.M. González-Casado, O. Vadillo, M.A. Rodríguez-Pascua, J.I. Cicuéndez, A. Casas, L. Cabañas, P. Rincón, A.L. Cortés, M. Ramírez and M. Lucini (2000). The recent (upper Miocene to Quaternary) and present tectonic stress distributions in the Iberian Peninsula, Tectonics 19 (4), 762-786; doi:10.1029/2000TC900006.

ICA (2011). Mapa de Andalucía Vectorial 1:10000, Instituto de Cartografía de Andalucía, Junta de Andlucía, Line@ online map database, version 1, http://juntadeandalucia.es/viviendayordenacion delterretorio/linea/, last access November 16, 2011, now offline, continued in version 2 by IECA (2013).

IECA (2013). Modelos digitales de Andalucía 10 metros/pixel, Instituto de Estadística y Cartografía de Andalucía, Line@ online map database, version 2, http://www.juntadeandalucia.es/institutodeestadisticaycartografia/lineav2/web/, last access May 22, 2013.

Keller, E., C. Sanz de Galdeano and J. Chacón (1996). Tectonic geomorphology and earthquake hazard of Sierra Nevada, Southern Spain, in 1 Conferencia Internacional Sierra Nevada, 20-22 March 1996, Granada, 201-218.

Keller, E., and N. Pinter (2002). Active tectonics: earthquakes, uplift, and landscape, 2nd edition, Prentice Hall, 122-150.

Kirby, E., and K. Whipple (2001). Quantifying differential rock-uplift rates via stream profile analysis, Geology, 29 (5), 415-418; doi:10.1130/0091-7613(2001)029<0415:QDRURV>2.0.CO;2.

Larue, J.P. (2008). Effects of tectonics and lithology on long profiles of 16 rivers of the southern Central Massif border between the Aude and the Orb (France), Geomorphology, 93 (3-4), 343-367; doi:10.1016/j.geomorph.2007.03.003.

Martínez-Martínez, J.-M., G. Booth-Rea, J.M. Azañón and F. Torcal (2006). Active transfer fault zone linking a segmented extensional system (Betics, southern Spain): Insight into heterogeneous extension driven by edge delamination, Tectonophysics, 422

(1-4), 159-173; doi:10.1016/j.tecto.2006.06.001.

Mezcua, J., J. Rueda and R.M. García Blanco (2013). Iberian Peninsula Historical Seismicity Revisited: An Intensity Data Bank, Seismological Research Letters, 84 (1), 9-18; doi:10.1785/0220120097.

Michetti, A.M., F.A. Audemard M. and S. Marco (2005). Future trends in paleoseismology: Integrated study of the seismic landscape as a vital tool in seismic hazard analyses, Tectonophysics, 408 (1-4), 3-21; doi:10.1016/j.tecto.2005.05.035.

Morales, J., I. Serrano, A. Jabaloy, J. Galindo-Zaldívar, D. Zhao, F. Torcal, F. Vidal, F. Lodeiro and F. González-Lodeiro (1999). Active continental subduction beneath the Betic Cordillera and the Alboran Sea, Geology, 27 (8), 735-738; doi:10.1130/0091-7613(1999)027<0735:ACSBTB>2.3.CO;2.

Muñoz, D., A. Cisternas, A. Udías, J. Mezcua, C. Sanz de Galdeano, J. Morales, M. Sánchez-Venero, H. Haessler, J. Ibañez, E. Buforn, G. Pascual and L. Rivera (2002). Microseismicity and tectonics in the Granada Basin (Spain), Tectonophysics 356, 233-252.

Peláez Montilla, J.A., C. Sanz de Galdeano and C. López Casado (2001). Seismic potential of faults in the Granada Basin (Betic Cordillera, Spain), Bulletin of the Geological Society of Greece, 34 (4), 1595-1600.

Pérez-Peña, J.V., A. Azor, J.M. Azañón and E.A. Keller (2010). Active tectonics in the Sierra Nevada (Betic Cordilleras, SE Spain): Insights from geomorphic indexes and drainage pattern analysis, Geomorphology, 119, 74-87; doi:10.1016/j.geomorph.2010.02.020.

Reicherter, K.T. Pletsch, W. Kuhnt, J. Manthey, G. Homeier, J. Wiedmann and J. Thurow (1994). Mid-Cretaceous paleogeography and paleoceanography of the Betic Seaway (Betic Cordillera, Spain), Palaeogeography, Palaeoclimatology, Palaeoecology, 107 (1), 1-33; doi:10.1016/0031-0182(94)90162-7.

Reicherter K. (2001). Paleoseismologic advances in the Granada basin (Betic Cordilleras, Southern Spain), Acta Geologica Hispanica, 36 (3-4), 267-281.

Reicherter K., A. Jabaloy, J. Galindo-Zaldívar, P. Ruano, P. Becker-Heidmann, J. Morales, S. Reiss and F. González-Lodeiro (2003). Repeated palaeoseismic activity of the Ventas de Zafarraya fault (S Spain) and its relation with the 1884 Andalusian earthquake, International Journal of Earth Sciences, 92 (6), 912-922; doi:10.1007/s00531-003-0366-3.

Reicherter, K., and G. Peters (2005). Neotectonic evolution of the Central Betic Cordilleras (Southern Spain), Tectonophysics, 405 (1-4), 191-212; doi:10.1016/j.tecto.2005.05.022.

Riley, C., and J.M. Moore (1993). Digital elevation modeling in a study of the neotectonic geomorphology of the Sierra Nevada, southern Spain, Zeitschrift für Geomorphologie, Suppl. 94, 25-39.

Rockwell, T., E.A. Keller and D.L. Johnson (1985). Tectonic geomorphology of alluvial fans and mountain fronts near Ventura, California, In: M. Morisawa (ed.), Tectonic Geomorphology, Proceedings of the 15th Annual Geomorphology Symposium, Allen and Unwin Publishers, Boston, 183-207.

Ruiz, A.M., G. Ferhat, P. Alfaro, C. Sanz de Galdeano, M.C. de Lacy, G. Rodríguez-Caderot and A.J. Gil (2003). Geodetic measurements of crustal deformation on NW-SE faults of the Betic Cordillera, southern Spain, 1999-2001, Journal of Geodynamics, 35, 259-272.

Ruiz, A.M., J.J. Sousa, R.F. Hanssen, Z. Perski, L. Bastos and A.J. Gil (2007). Deformation in the Granada Basin (southern Betic Cordillera) studies by PS-INSAR: preliminary results, In: Proceedings of the Envisat Symposium 2007 (Montreux, Switzerland, April 23-27, 2007).

Sanz de Galdeano, C., J. González Donoso and J. Gallegos (1975). Mapa Geológico de España - 1026 Padul, Instituto Geológico y Minero de España.

Sanz de Galdeano, C. (1990). Geologic evolution of the Betic Cordilleras in the Western Mediterranean, Miocene to present, Tectonophysics, 172, 107-119; doi:10.1016/0040-1951(90)90062-D.

Sanz de Galdeano, C., and A. López-Garrido (1999). Nature and impact of the Neotectonic deformation in the western Sierra Nevada (Spain), Geomorphology, 30, 259-272; doi:10. 1016/S0169-555X(99)00034-3.

Sanz de Galdeano, C., J.A. Peláez and C. López Casado (2003). Seismic Potential of the Main Active Faults in the Granada Basin (Southern Spain), Pure and Applied Geophysics, 160 (8), 1537-1556; doi:10.1007/s00024-003-2359-3.

Sanz de Galdeano, C., and P. Alfaro (2004). Tectonic significance of the present relief of the Betic Cordillera, Geomorphology, 63, 175-190; doi:10.1016/j.geomorph.2004.04.002.

Sanz de Galdeano, C., and J.A. Peláez (2010a). Padul Fault (ES666), In: García-Mayordomo et al. (eds.), Quaternary Active Faults Database of Iberia v.2.0, IGME, Madrid.

Sanz de Galdeano, C., and J.A. Peláez (2010b). Padul-Dúrcal Fault (ES669), In: García-Mayordomo et al. (eds.), Quaternary Active Faults Database of Iberia v.2.0, IGME, Madrid.

Silva, P.G., J.L. Goy, C. Zazo and T. Bardají (2003). Fault-generated mountain fronts in southeast Spain: geomorphologic assessment of tectonic and seismic activity, Geomorphology, 50, 203-225; doi:10.1016/S0169-555X(02)00215-5.

Vissers, R.L.M., J.P. Platt and D. van der Wal (1995).

Late orogenic extension of the Betic Cordillera and the Alboran Domain: A lithospheric view, Tectonics, 14 (4), 786-803; doi:10.1029/95TC00086.

Weijermars, R. (1991). Geology and tectonics of the Betic Zone, SE Spain, Earth-Science Reviews, 31, 153-236; doi:10.1016/0012-8252(91)90019-C.

Wells, S.G., T.F. Bullard, C.M. Menges, P.G. Drake, P.A. Karas, K.I. Kelson, J.B. Ritter and J.R. Wesling (1988). Regional variations in tectonic geomorphology along a segmented convergent plate boundary pacific coast of Costa Rica, Geomorphology, 1 (3), 239-265; doi:10.1016/0169-555X(88)90016-5.

Wells, D.L., and K.J. Coppersmith (1994). New Empirical Relationships among Magnitude, Rupture Length, Rupture Width, Rupture Area, and Surface Displacement, Bulletin of the Seismological Society of America, 84 (4), 974-1002.

*Corresponding author: Andreas Rudersdorf,
RWTH Aachen University, Neotectonics and Natural Hazards,
Aachen, Germany; email: a.rudersdorf@nug.rwth-aachen.de.